

## Detection and interpretation of precursory magnetic signals preceding October 30, 2020 Samos earthquake

İlkin ÖZSÖZ<sup>1\*</sup>, Oya ANKAYA PAMUKÇU<sup>2</sup>

<sup>1</sup>General Directorate of Mineral Research and Exploration, Ankara

<sup>2</sup>Dokuz Eylül University, Engineering Faculty, Geophysical Engineering, İzmir

Received: 11.07.2021 • Accepted/Published Online: 17.10.2021 • Final Version: 30.10.2021

**Abstract:** A major earthquake ( $M_w=7.0$ ) occurred in the Samos Island on the 30th of October 2020 at 11:51 UTC. Swarm satellite magnetic data were analysed for 153 days before and 46 days after the earthquake. Preearthquake and postearthquake anomaly search is constrained within the Dobrovolsky's Circular Area. Fundamentally, there are 5 steps for processing satellite magnetic data to interpret the earthquake preparation phase. The first step is converting geographical coordinates to geomagnetic latitude and longitude. Secondly, intensity of the external magnetic field should be evaluated by magnetic indices ( $A_p$ ,  $K_p$  and  $|Dst|$ ). Thirdly, preearthquake and postearthquake magnetic anomaly should be constrained through magnetic indices ( $A_p < 20$ ,  $K_p \leq 3$  and  $|Dst| < 10$ ) and Dobrovolsky's Circular Area. The following step is filtering short-wavelength magnetic anomalies using first time derivative and trend removal (de-trend). Finally, anomalous residual magnetic variations of the satellite tracks are classified through RMS analysis. The cumulative number of anomalous points (y-axis) is plotted versus the date (x-axis).  $R^2$  values denote the degree of linear distribution of the anomalous tracks. For X, Y, Z, and F components of the magnetic field,  $R^2$  is computed as 0.9038, 0.8697, 0.8490, and 0.9694, respectively. Y component of the magnetic field provided the best results in terms of interpretation. Regarding the results of the Y component, linear distribution and deviation from this distribution are fairly distinguishable.

**Key words:** Satellite magnetic data, precursory earthquake signals, Swarm satellite constellation, magnetic field components, Samos 2020 earthquake

### 1. Introduction

The major target of the precursory earthquake studies is revealing time-dependence behaviour of the seismic activity. Physical and statistical earthquake forecasting models possibly shed light on natural seismic activity and aftershock triggering. Moreover, historical seismicity of a region may help to estimate future earthquakes. The current precursory earthquake studies are suffering from precise estimation of short-term seismicity. Even though precursory earthquake analysis lack of projecting near future earthquakes, it has a significant potential to reduce earthquake losses (Jordan et al., 2011).

Lithospheric-asthenospheric-ionospheric coupling (LAIC) can be defined as geophysical and geochemical variations on the lithosphere, asthenosphere, and ionosphere (Pulinets et al., 2011; Pulinets et al., 2015). LAIC model was firstly defined by Pulinets et al. (1994) who analysed aerosols, natural radioactivity, and ionospheric electricity to demonstrate seismo-ionospheric variations.

There are many studies that indicate LAIC anomalies during the earthquake preparation phase (Parrot, 1995;

Troyan and Hayakawa, 2002; Tronin et al., 2002; Pulinets et al., 2011; De Santis et al., 2015; Pulinets et al., 2015; Akhoondzadeh et al., 2018). Marchetti and Akhoondzadeh (2018) used magnetic scalar and vectors (X, Y, Z and F) with electron density and temperature to monitoring anomalies before the  $M_w = 8.2$  Mexico earthquake.

Marchetti et al. (2020) linked magnetic anomalies to seismicity 40 days before the beginning of the seismic sequence. De Santis et al. (2019) detected magnetic and electron density anomalies of 12 strong earthquakes by comprehensive statistical analysis. Furthermore, LAIC was modelled in terms of the emission of radioactive gas and metallic ions (Freund, 2011). Sorokin et al. (2001) suggested that electrical potential above Earth's surface and ionosphere vary before a massive earthquake. Akhoondzadeh (2011) used multiprecursor techniques for 16 April 2016-M7.8 Ecuador earthquake.

A major earthquake ( $M_w = 7.0$ ) is recorded in the northern part of the Samos (October 30, 2020) in the Eastern Aegean Sea. The earthquake caused the death of 117 people in Turkey and Greece due to the building

\* Correspondence: [ilkin.ozsoz@mta.gov.tr](mailto:ilkin.ozsoz@mta.gov.tr)

collapse. Additionally, approximately 1030 injuries were reported. After the earthquake, ground fractures and coastal uplifts were observed (Mavroulis et al., 2021). Southwest coast of İzmir and Samos Island was hit by a moderate tsunami (Dogan et al., 2021; Triantafyllou et al., 2021). The focal depth of the earthquake was estimated at 21 km<sup>1</sup>. Samos earthquake has been investigated by many researchers (Aksoy, 2021; Fomelis et al., 2021; Ganas et al., 2021; Karakostas et al., 2021; Kaviris et al., 2021; Kourouklas et al., 2021; Kouskouna, 2021; Oruç and Balkan, 2021; Vallianatos and Pavlou, 2021).

In this study, we investigated for magnetic precursory anomalies preceding the M = 7.0 Samos Earthquake, and we processed data from Swarm satellite covering 200 days.

The paper will focus on characteristics of magnetic anomaly before, during and after the October 30, 2020 Samos earthquake. In the following parts, a brief tectonic setting of the study area, Swarm and magnetic indices data explanation, methodology of the precursor earthquake anomaly detection, findings and qualitative and quantitative interpretation of the results will be evaluated.

Cretaceous aged Hellenide-Anatolide orogen formed in the southern margin of the Eurasia plate (Sengor and Yilmaz, 1981; Robertson and Dixon, 1984; Gessner, 2001). Alignment of the tectonic structures of the Hellenide-Anatolide orogen and Hellenic subduction zone are highly correlated (Brunn, 1956; Dürr et al., 1978). The simplified tectonic map of the area, which comprises Hellenide-Anatolide orogeny system and Hellenic subduction zone, is shown in Figure 1.

Median Crystalline Belt (Dürr et al., 1978) comprises the Paleogonian Zone, the Cycladic Zone and the Menderes Massif (Parejas et al., 1940). In general, the Median Crystalline Belt is specified by Carboniferous basement, and it is covered by Permo-Mesozoic Adriatic Plate (Gessner, 2001).

From top to bottom, Hellenides can be divided into the internal zone, the Vardar-İzmir-Ankara Zone, the Lycian Allochthon, the Cycladic Zone, and the external zone (Gessner, 2001).

Western Anatolia or Eastern Aegean region tectonic system is specified by extremely active extension and excessive seismic activity. Pamukçu and Yurdakul (2008) highlighted the relationship between focal depth and effective elastic thickness in Western Anatolia. Dogru et al. (2017) classified the ductile and brittle parts of the lithospheric crust via phase characteristics of the Bouguer anomaly data in terms of focal depths of the earthquakes. Oruç and Balkan (2021) used geoid undulations to interpret stress patterns in and around the Samos Island. According to their results, a notable stress increase was observed in around the Ikaria Island (Greece).

## 2. Data

The magnetic data used in this study have been obtained from the Swarm satellite constellation, which is a European Space Agency (ESA) mission that contains three identical satellites (Friis-Christensen et al., 2006). Three Swarm satellites, which are Alpha, Bravo, and Charlie, are identical and Alpha and Charlie are flying side-by-side with 1.4° longitude separation. The flying altitude of the Alpha and Charlie satellites is roughly 450 km. Furthermore, the Bravo satellite flies above 580 km.

Since there are three satellites, researchers can analyse small scale variations of the lithospheric magnetic field. The main sensors of the satellites used for measuring the geomagnetic field are the absolute scalar magnetometer (ASM) and vector field magnetometer (VFM). In this study, low resolution VFM Level 1B 1Hz data were used for earthquake precursor analysis from May 30, 2020 to December 15, 2020. It should be noted that ASM data for the Charlie (Swarm C) satellite are not available due to the problems after launch.

It is crucial that satellite magnetic data are affected by external sources. Therefore, geomagnetic indices ( $D_{st}$ ,  $K_p$  and  $A_p$ ) are used for distinguishing seismic anomalies from external sources associated with geomagnetic and solar activities. The geomagnetic indices are obtained from <https://omniweb.gsfc.nasa.gov/>.

## 3. Methods

In this study, the Magnetic Swarm Anomaly Detection by Spline analysis (MASS) has been applied to the low resolution VFM Level 1B 1Hz data. The applied method in this study is quite similar to the method proposed by De Santis et al. (2019).

Firstly, geographic coordinates are transformed into geomagnetic latitude and longitude through the geomagnetic North Pole. The total magnetic field component (F) is calculated from the other magnetic field components (X, Y and Z).

Then, the time of  $A_p$ ,  $K_p$  and  $|D_{st}|$  and Swarm magnetic data is matched via interpolation. The intensity of external magnetic sources is interpreted by these geomagnetic indices.

The relationship between seismic activity and magnetic anomalies should be analysed within the earthquake preparation area proposed by Dobrovolsky et al. (1979). Dobrovolsky's circle can be calculated by  $R_{DB} = 10^{0.43M}$  where  $R_{DB}$  is the radius of the circular preparation area, and M is the earthquake magnitude. The satellite tracks that fall within the Dobrovolsky's circular area are chosen.

The geomagnetic indices are used to detect periods with low magnetic activity between May 30, 2020 and

<sup>1</sup> U.S. Geological Survey (2020). Search Earthquake Catalog [online]. Website <https://earthquake.usgs.gov/earthquakes/search/> [accessed 12 December 2020].

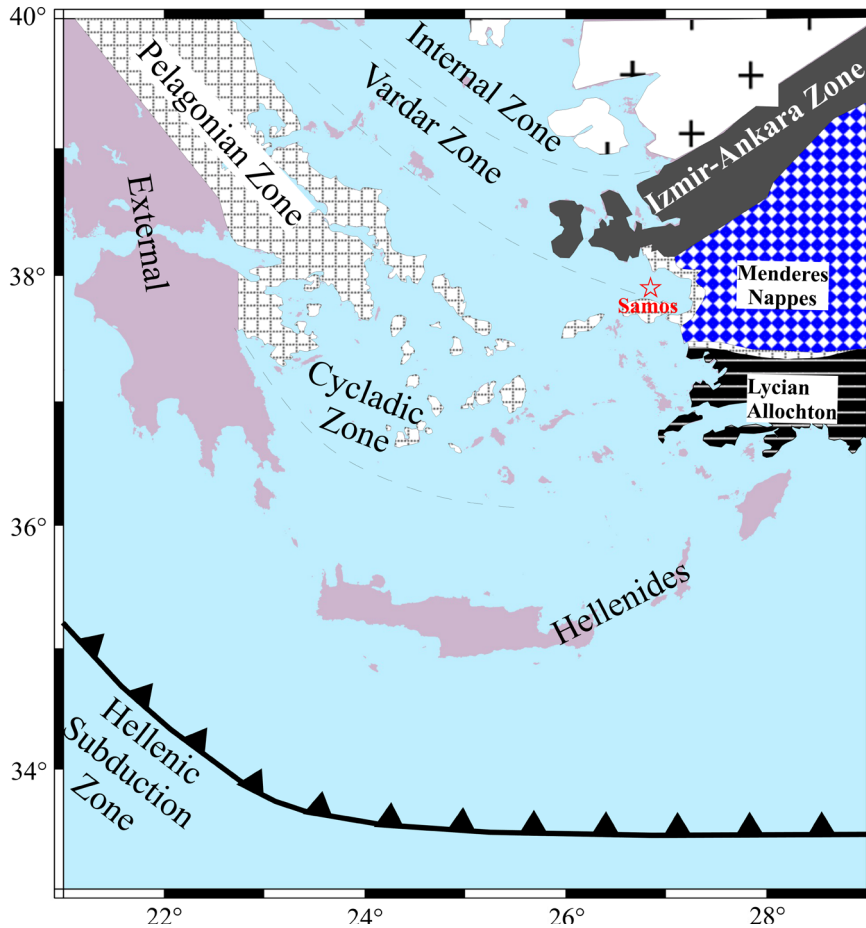


**Figure 1.** Simplified tectonic map of Samos and its surroundings (modified and simplified from Seidel et al., 1982; Schermer et al., 1990; Avigad et al., 1997; Walcott, 1998; Broecker and Enders, 1999; Ring et al., 2001; Gessner, 2001).

December 15, 2020. For this study, there are three geomagnetic indices:  $A_p$ ,  $K_p$ , and  $D_{st}$ . The  $A_p$  index provides a daily average level of geomagnetic activity while the  $K_p$  index describes disturbances of the geomagnetic field resulted from the solar wind. Finally, the  $D_{st}$  index, which was obtained by near equatorial magnetic observatories, presents the intensity of the ring current.

External sources of magnetic field produce anomalies that are not related to seismicity. Hence, the anomalies related to the external sources should be removed from the data by detecting quiet geomagnetic conditions. According to Marchetti et al. (2020),  $A_p > 20$  and  $|D_{st}| > 10$  represents geomagnetic disturbed time. Desler and Fejer (1963) suggested  $K_p$  higher than 3 indicates minor, moderate, and major auroral activity. Hence,  $A_p < 20$ ,  $K_p \leq 3$ , and  $|D_{st}| < 10$  are used as a threshold for the quiet geomagnetic conditions.

Firstly, the derivative is applied to the chosen satellite tracks. Then the tracks are undergone a de-trending process in order to remove variations associated with the

long wavelength component. The first time derivative and de-trending process removed the long term trend from the data. De-trending and first time derivative allow the interpreter to observe residual variations in the magnetic field components.

Since strict threshold values are used, the selected data is assumed to comprise regular trend of the magnetic field and fluctuations, associated with the seismic activity. In this paper, the term “anomaly” refers to disturbances in the first derivative of the de-trended and filtered magnetic data for a single satellite tracks due to the precursory earthquake signals. Moreover, anomalous tracks can be defined as the satellite tracks that include the seismo-magnetic anomalies.

Each satellite track should be analysed separately in terms of the number of anomalous tracks. There are 482 tracks within the Dobrovolsky’s area. Manual searching of the anomalous period would be quite time-consuming and subjective. Consequently, an autonomous searching method via the RMS window is used.

The anomalous tracks were detected by moving the RMS window. RMS of the whole track ( $DATA_{RMS}$ ) is compared to the RMS of the windowed data ( $WINDOW_{RMS}$ ). If  $WINDOW_{RMS} > DATA_{RMS}$ , the track is considered as anomalous, whereas the track is interpreted as not-anomalous where  $WINDOW_{RMS} < DATA_{RMS}$ . The anomalous tracks are plotted with respect to the studied period expressed in days.

#### 4. Results and interpretation

The reliability of results is dependent on how successfully external sources are removed using geomagnetic indices. The interpolated hourly  $D_{st}$  and  $K_p$  and 3 hourly  $a_p$  are plotted against the relative time with respect to the earthquake dated October 30, 2020. (Figure 2).

The irregular variations of the magnetic field variations result from the interaction of the solar wind with the ionosphere and magnetosphere. The geomagnetic indices provide information to resolve irregular diurnal magnetic activity.

In Figure 2, the 3-hourly variation of  $K_p$  index is based on measurements by 13 magnetic observatories. The index is presented according to the practice by Bartels (1949). The index, ranging from 0 to 9, denotes the level of the disturbance of the geomagnetic field by the solar wind. If  $K_p$  is less than or equal to 3, it is interpreted as quiet geomagnetic conditions. On the other hand, values of  $3 < K_p < 7$  corresponds to the minor or moderate solar wind. However,  $K_p \geq 7$  indicates strong and intense geomagnetic storms. In this study,  $K_p \leq 3$  is used to filter minor, moderate, and intense geomagnetic storms.

The  $|D_{st}|$  index (Sugira and Poros, 1971) is measured hourly, and it reveals low latitude horizontal irregular magnetic activities. In other words, the index presents the ring currents (symmetrical equatorial electrojet). During large solar storms, the H component of the magnetic field deviates from the general trend.

Similar to the  $K_p$  index, the  $A_p$  (Rostoker, 1972; Mayaud et al., 1980) index is measured on 3-hourly basis. The index provides general information about geomagnetic storms, since 3-hourly measured data are processed by an 8-point running average.

Overall, the anomalous period can be described between day -20 and day -40 since  $K_p$ ,  $|D_{st}|$  and  $A_p$  are fairly anomalous. As it was mentioned before,  $A_p < 20$ ,  $K_p \leq 3$  and  $|D_{st}| < 10$  thresholds were used for selection of the satellite magnetic data.

To determine the radius of the study area, the Dobrovolsky's area provides a reasonable approximation (Vizzini and Brai, 2012). Results of the statistical analysis are considerably dependent on the number of satellite tracks within the Dobrovolsky's area. Figure 3 demonstrates the distribution of the satellite tracks and Dobrovolsky's circular area, which is of a radius of 1003.44 km.

As it can be seen from Figure 3, Dobrovolsky's area covers a large region. For the earthquake precursory analysis, satellite trajectories within the Dobrovolsky's zone are used. It can be said that the majority of the satellite trajectories are aligned along about N-S trend. Qualitatively, it can be said that coverage of the satellite tracks is adequate.

The single track analysis within the Dobrovolsky's area is illustrated in Figure 4. De-trend is applied for the first time, and the derivatives of each magnetic component (X, Y, Z and F) are plotted ( $dX/dT$ ,  $dY/dT$ ,  $dZ/dT$  and  $dF/dT$ ). The magnetic components recorded on September 22<sup>nd</sup> occurred between 04:23 a.m. and 04:33 a.m. The time period corresponds from 6.55 to 6.95 for magnetic local time (MLT).

It can be said that there are no anomalies on X, Z and F components for this track. However, one anomalous period is detected on the Y component within the Dobrovolsky's area.

In Figure 5, the cumulative number of the anomalous track is compared to the linear model. Deviations from the linear fit can be interpreted as how preearthquake and postearthquake processes affected the magnetic components. In order to analyse these deviations quantitatively,  $R^2$  values are used.  $R^2$  indicates the correlation between the X and Y axes. Namely, if observations are completely linear,  $R^2$  will be 1.

Regarding the interpretation of the  $B_x$  component, it can be said that almost all data points follow a linear trend (Figure 6). Furthermore,  $R^2$  is roughly 0.90, which indicates a nearly linear trend. Before the seismic event, the increase in the number of anomalous tracks is quite stable. However, slight deviations from the linear trend are observed shortly after October 30, 2020. At the beginning of October, the number of anomalous tracks started to rise remarkably.

Moreover, the  $B_y$  component presents irregular variations respect to the linear fit (Figure 7). The irregular behaviour can be quantitatively observed from the  $R^2$  value, which is 0.8697. Even though the general increasing rate of the number of anomalous tracks is unstable, the distribution is quite linear until the beginning of October. After the mainshock, postearthquake trend is observed end of the S-shaped trend. Roughly one month before the major earthquake, the position of the anomalous trend notably deviates from the linear trend.

The  $B_z$  component of the magnetic field cannot produce statistically reliable results due to the few data points (Figure 8).  $B_z$  component has the smallest  $R^2$  value for 5 data points. From the beginning of August to September 2021, the number of anomalous tracks increased gradually. Shortly before the mainshock, the detected number of anomalous tracks through the autonomous searching

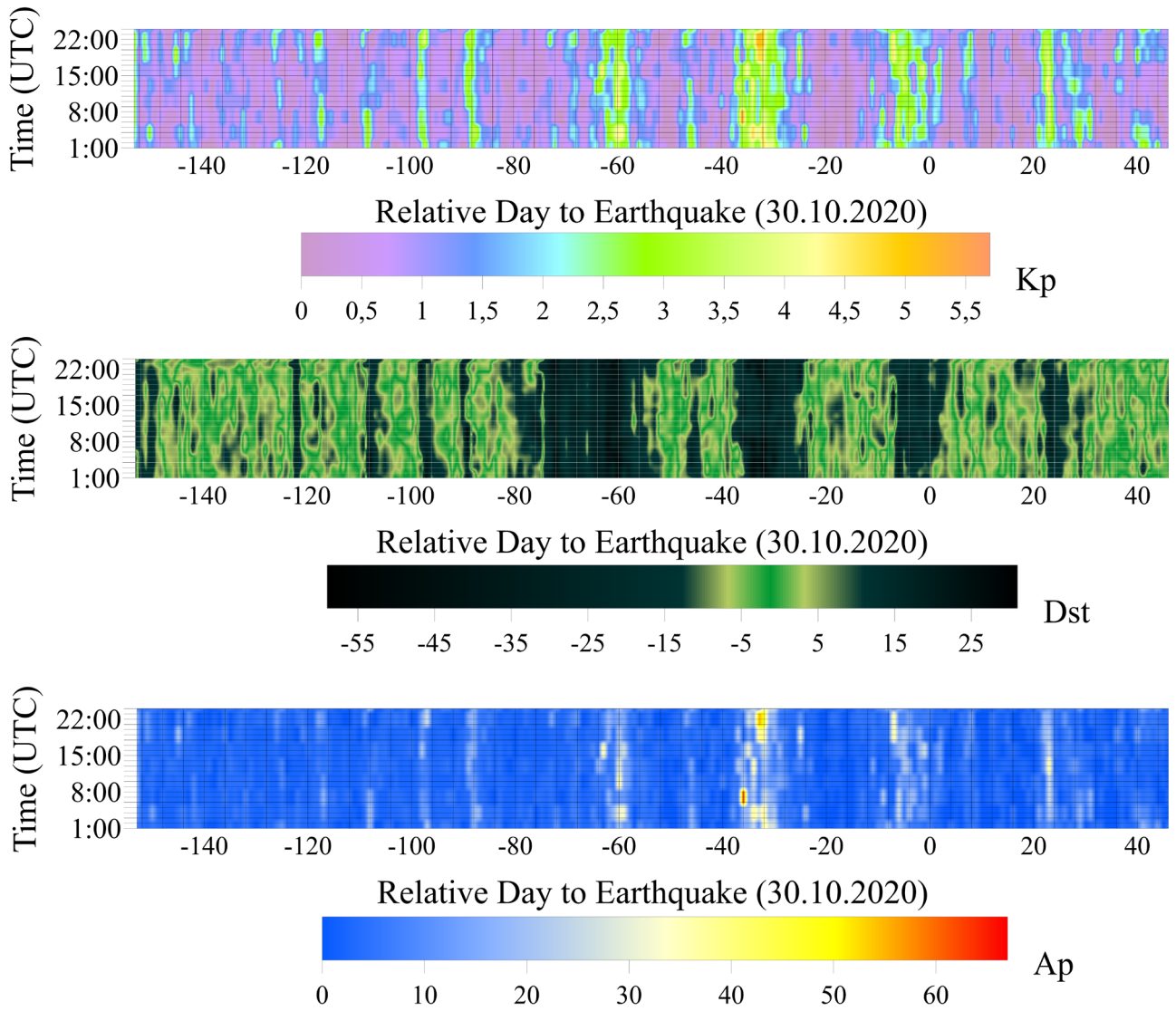


**Figure 2.** Map of hourly (or 3 hourly) geomagnetic indices against the relative day to earthquake.

method decreased. Immediately after the seismic event, a considerable increase of the anomalous points is observed. It should be noted that there is only one point after the main earthquake event. For reliable interpretation, more points are required.

The total magnetic field component (Figure 9),  $F$ , is almost linear. Additionally, it has the highest  $R^2$  value, which proves the linear behaviour quantitatively. The deviation from the linear fit is notably small. The trend of the cumulative number of anomalous tracks converged to the linear model after the earthquake.

For a single satellite track, longer wavelengths of the magnetic field that are observed in the geomagnetically quiet period tend to follow a linear trend. However, precursory signals of the earthquake generate magnetic disturbances (anomalies) in the linear trend (Figure 4).

On the whole, the S-shaped anomaly is considerably remarkable on Y magnetic component. The S-shaped anomaly starts with a linear trend until the earthquake. After the seismic event, postearthquake trend starts. The best evaluation of the lithospheric variations can be interpreted from  $B_y$ .

### 5. Conclusion

Preearthquake and postearthquake variations should be interpreted on the basis of the distribution of the anomalous data. In general, preearthquake data are specified by linear characteristics. Then, a different trend is observed on the post-earthquake data. The S-shaped curve is noted for the X, Y, Z, and F magnetic components. Consequently, the S-shaped curve (Akhoondzadeh et al., 2018; Marchetti, and Akhoondzadeh, 2018; De Santis et

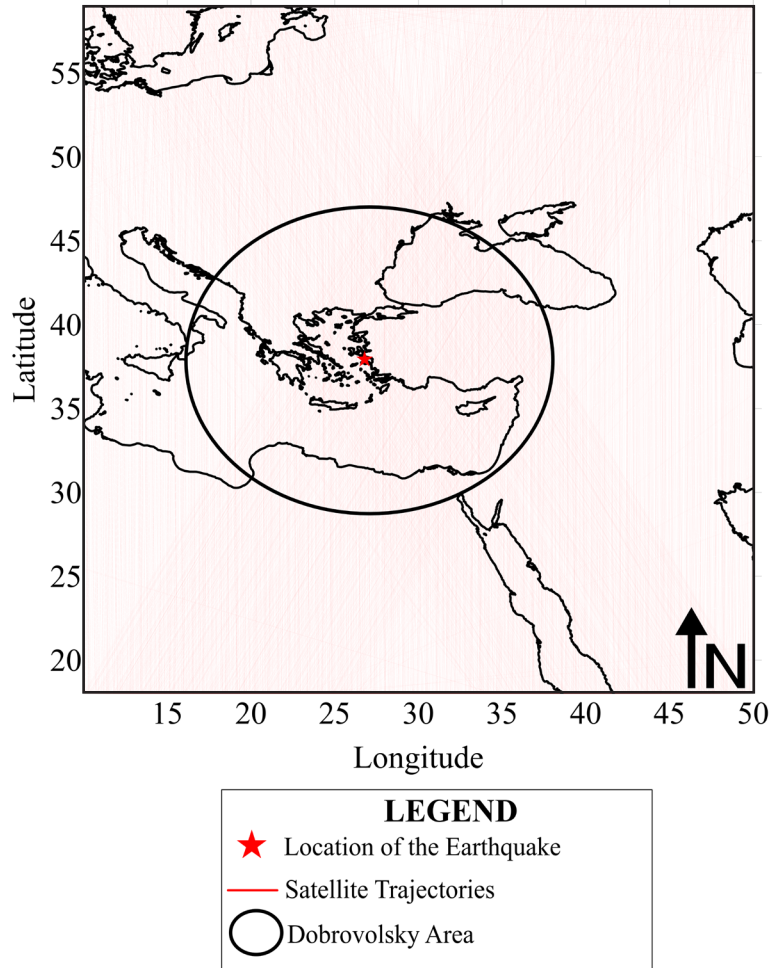


Figure 3. Satellite trajectories and Dobrovolsky's circular area for this study.

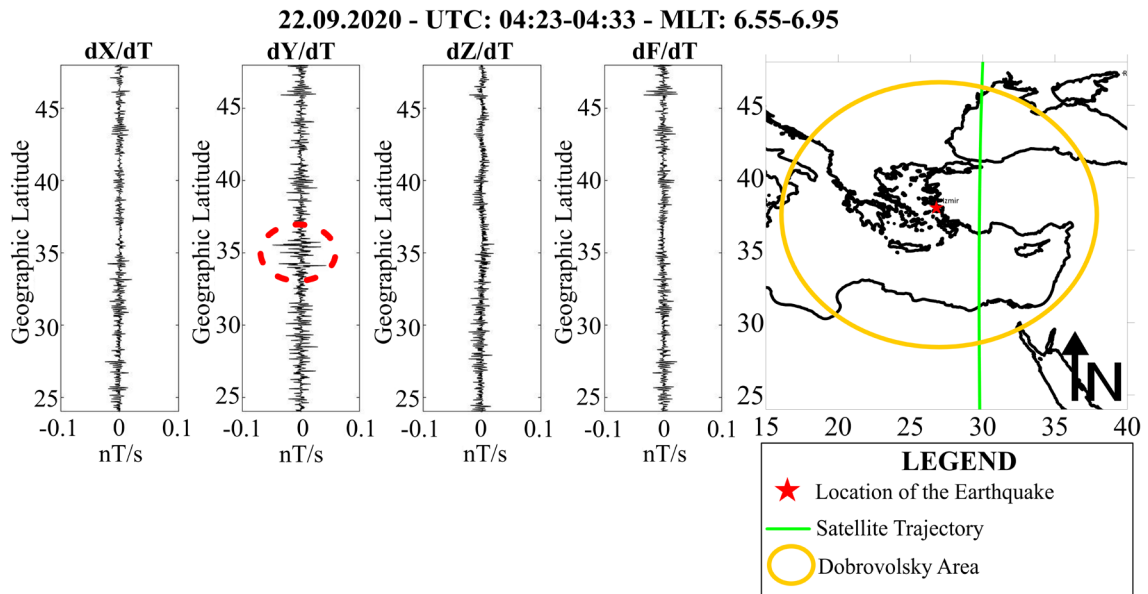
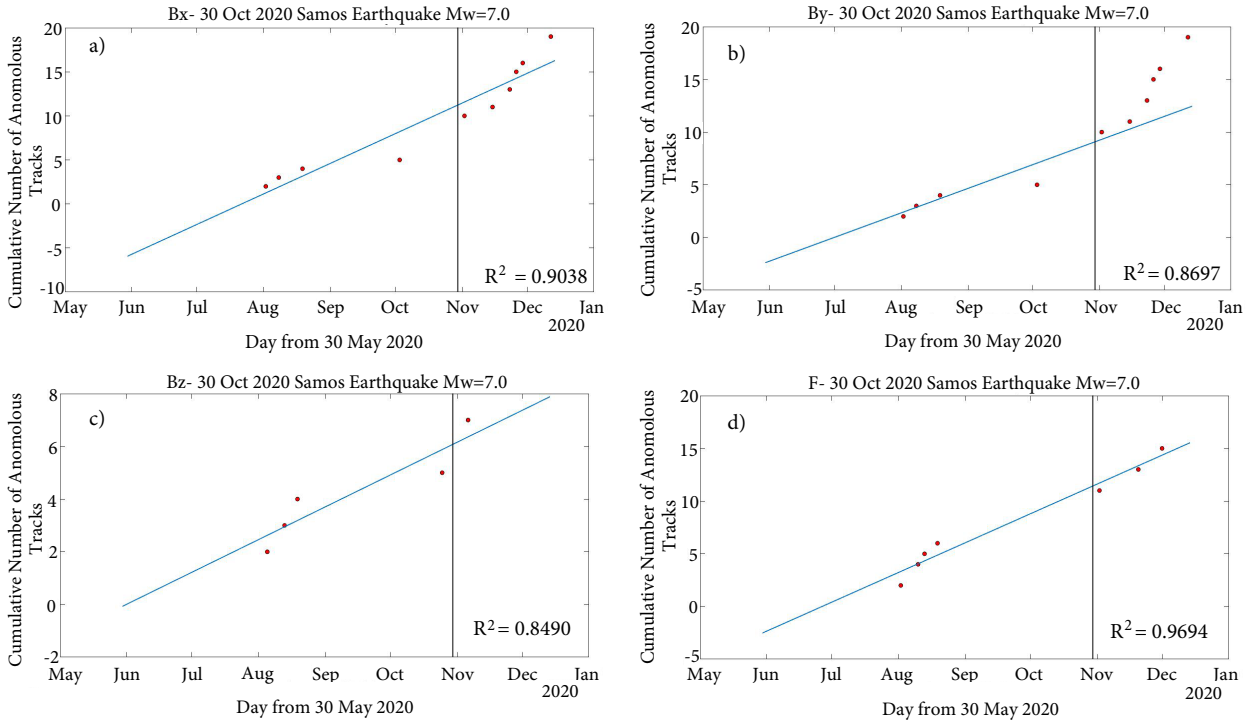
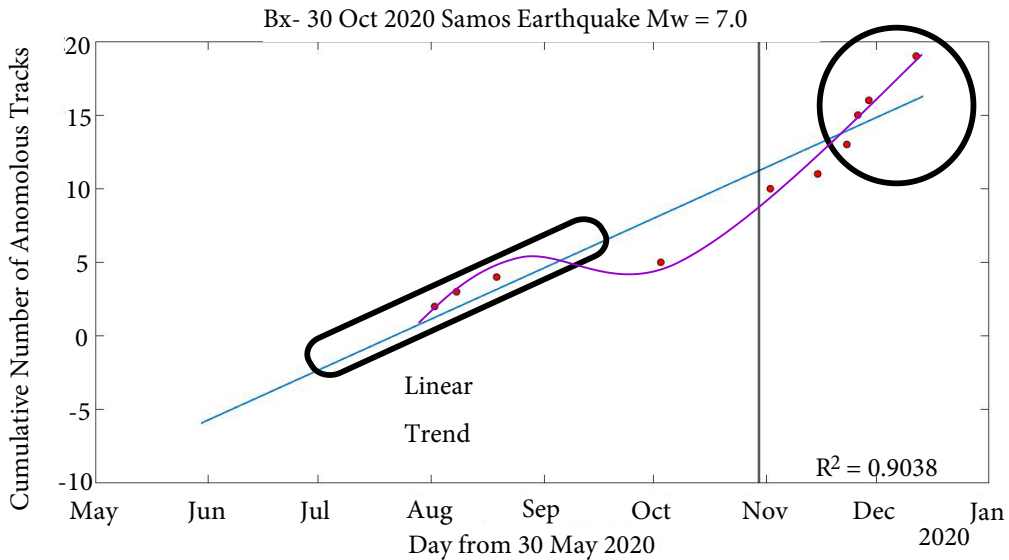


Figure 4. Anomalous magnetic anomaly during the earthquake preparation phase. The anomalous period is denoted by the red circle for  $dY/dT$ .



**Figure 5.** The cumulative number of anomalous tracks for a) Bx, b) By c) Bz and d) F components. The day of the seismic event (30.10.2020) is denoted by the vertical black line.



**Figure 6.** Diagram of X component of the magnetic field.

al., 2019; Zhu et al., 2019; Marchetti et al., 2020). can be evaluated as a precursory earthquake signal.

The best response is obtained from the Y component of the magnetic field in terms of the anomalous tracks. Before the main shock (black line), the anomalous tracks distributed around the linear fit (blue line). Then, roughly one month before the main earthquake, there is a

considerable deviation from the trend. After October 30, 2020, notable variations from the pre-earthquake linear trend initiated.

The observations for  $B_y$  about the anomalous tracks are also valid for the  $B_x$  component, but the rate of change is fairly weaker than the  $B_y$  component. The spatial distribution of the anomalous tracks in the  $B_x$  component ( $R^2 = 0.9038$ ) is

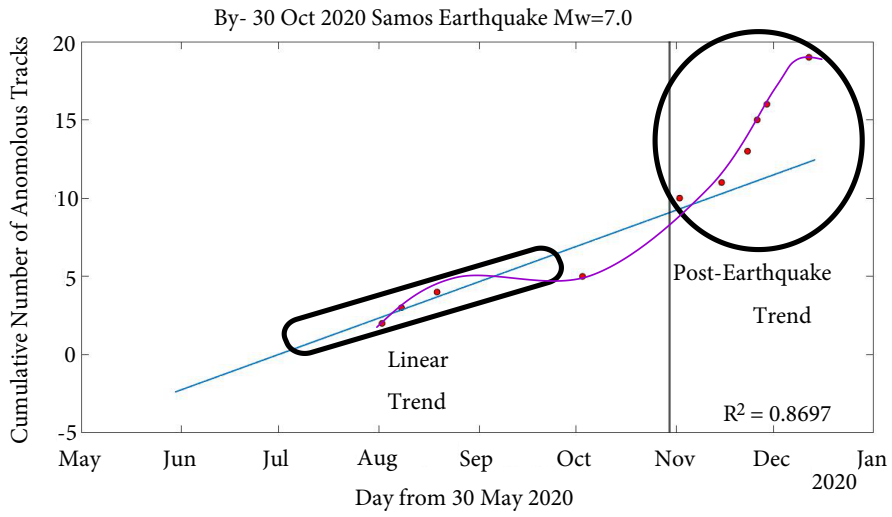


Figure 7. Diagram of Y component of the magnetic field.

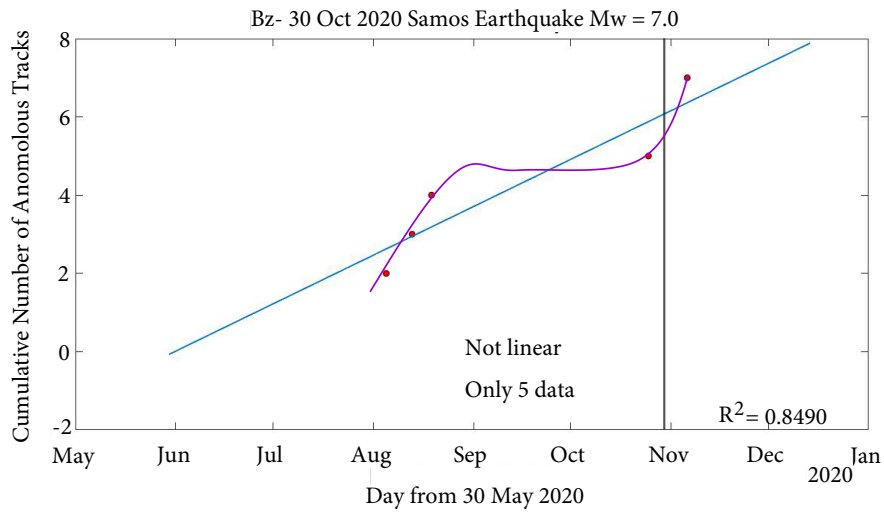


Figure 8. Diagram of Z component of the magnetic field.

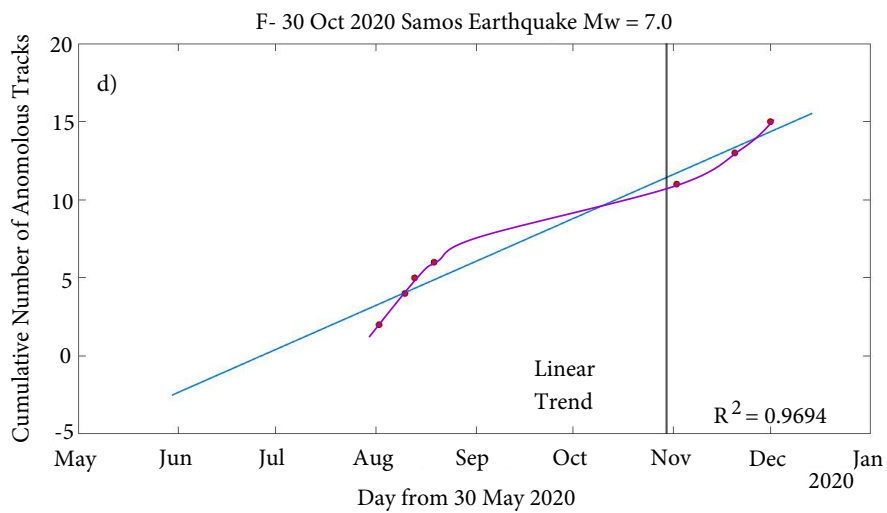


Figure 9. Diagram of F component of the magnetic field.

notably linear rather than the  $B_y$  component ( $R^2 = 0.8697$ ).

Results of the  $B_z$  component is not reliable and interpretable, since there are only 5 anomalous tracks

are detected. Furthermore, the rate of change in the F component is dramatically weak, and detected anomalous tracks are almost linear ( $R^2 = 0.9694$ ).

## References

- Akhoondzadeh M (2011). Comparative study of the earthquake precursors obtained from satellite data. PhD. University of Tehran, Tehran, Iran.
- Akhoondzadeh M, De Santis A, Marchetti D, Piscini A, Cianchini G (2018). Multi precursors analysis associated with the powerful Ecuador (MW= 7.8) earthquake of 16 April 2016 using Swarm satellites data in conjunction with other multi-platform satellite and ground data. *Advances in Space Research* 61 (1): 248-263. doi: 10.1016/j.asr.2017.07.014
- Bartels J (1949). The standardized index,  $K_s$ , and the planetary index,  $K_p$ . *International Association of Geomagnetism and Aeronomy Bulletin* 97 (12b): 0001.
- Broecker M, Enders M (1999). U–Pb zircon geochronology of unusual eclogite-facies rocks from Syros and Tinos (Cyclades, Greece). *Geological Magazine* 136 (2): 111-118. doi: 10.1017/S0016756899002320
- Avigad D, Garfunkel Z, Jolivet L, Azañón JM (1997). Back arc extension and denudation of Mediterranean eclogites. *Tectonics* 16 (6): 924-941. doi: 10.1029/97TC02003
- Brunn JH (1956). Contribution à l'étude du Pinde septentrional et d'une partie de la Macédoine occidentale. *Annales Géologiques du Pays Helléniques* 7: 1-358 (in French with English abstract).
- De Santis A, De Franceschi G, Spogli L, Perrone L, Alfonsi L et al. (2015). Geospace perturbations induced by the Earth: The state of the art and future trends. *Physics and Chemistry of the Earth Parts A/B/C* 85: 17-33. doi: 10.1016/j.pce.2015.05.004
- De Santis A, Marchetti D, Spogli L, Cianchini G, Pavón-Carrasco FJ et al. (2019). Magnetic field and electron density data analysis from swarm satellites searching for ionospheric effects by great earthquakes: 12 Case studies from 2014 to 2016. *Atmosphere* 10 (7): 371. doi: 10.3390/atmos10070371
- Dessler AJ, Fejer JA (1963). Interpretation of  $K_p$  index and M-region geomagnetic storms. *Planetary and Space Science* 11 (5): 505-511. doi: 10.1016/0032-0633(63)90074-6
- Dobrovolsky IP, Zubkov SI, Miachkin VI (1979). Estimation of the size of earthquake preparation zones. *Pure and Applied Geophysics* 117 (5): 1025-1044. doi: 10.1007/BF00876083
- Freund F (2011). Pre-earthquake signals: Underlying physical processes. *Journal of Asian Earth Sciences* 41 (4-5): 383-400. doi: 10.1016/j.jseaes.2010.03.009
- Dogan GG, Yalciner AC, Yuksel Y, Ulutaş E, Polat O et al. (2021). The 30 October 2020 Aegean Sea Tsunami: Post-Event Field Survey Along Turkish Coast. *Pure and Applied Geophysics* 178 (3): 785–812. doi: 10.1007/s00024-021-02693-3
- Dogru F, Pamukcu O, Ozsoz I (2017). Application of tilt angle method to the Bouguer gravity data of Western Anatolia. *Bulletin of the Mineral Research and Exploration* 155 (155): 213-222. doi: 10.19111/bulletinofmre.305177
- Dürr S (1978). The median Aegean crystalline belt: stratigraphy structure, metamorphism, magmatism.
- Foumelis M, Papazachos C, Papadimitriou E, Karakostas V, Ampatzidis D et al. (2021). On rapid multidisciplinary response aspects for Samos 2020 M7. 0 earthquake. *Acta Geophysica* 1-24. doi: 10.1007/s11600-021-00578-6
- Friis-Christensen E, Lühr H, Hulot G (2006). Swarm: A constellation to study the Earth's magnetic field. *Earth, planets and space* 58 (4): 351-358. doi: 10.1186/BF03351933
- Ganas A, Elias P, Briole P, Valkaniotis S, Escartin J et al. (2021). Co-seismic and post-seismic deformation, field observations and fault model of the 30 October 2020 Mw= 7.0 Samos earthquake, Aegean Sea. *Acta Geophysica*, 1-26. doi: 10.1007/s11600-021-00599-1
- Gessner K, Ring U, Passchier CW, Güngör T (2001). How to resist subduction: evidence for large-scale out-of-sequence thrusting during Eocene collision in western Turkey. *Journal of the Geological Society* 158 (5): 769-784. doi: 10.1144/jgs.158.5.769
- Jordan TH, Chen YT, Gasparini P, Madariaga R, Main I et al. (2011). Operational earthquake forecasting. State of knowledge and guidelines for utilization. *Annals of Geophysics* 54 (4). doi: 10.4401/ag-5350
- Karakostas V, Tan O, Kostoglou A, Papadimitriou E, Bonatis P (2021). Seismotectonic implications of the 2020 Samos, Greece, Mw 7.0 mainshock based on high-resolution aftershock relocation and source slip model. *Acta Geophysica*, 1-18. doi: 10.1007/s11600-021-00580-y
- Kaviris G, Spingos I, Kapetanidis V, Papadimitriou P, Voulgaris, N (2021). On the origin of upper crustal shear-wave anisotropy at Samos Island, Greece. *Acta Geophysica* 1-14. doi: 10.1007/s11600-021-00598-2
- Kourouklas C, Mangira O, Console R, Papadimitriou E, Karakostas V et al. (2021). Short-term clustering modeling of seismicity in Eastern Aegean Sea (Greece): a retrospective forecast test of the 2017 M w= 6.4 Lesvos, 2017 Mw= 6.6 Kos and 2020 M w= 7.0 Samos earthquake sequences. *Acta Geophysica* 1-15. doi: 10.1007/s11600-021-00583-9
- Kouskouna V (2021). Updating the macroseismic intensity database of 19th century damaging earthquakes in Greece: a case study in Samos Island. *Acta Geophysica* 1-11. doi: 10.1007/s11600-021-00608-3

- Marchetti D, Akhoondzadeh M (2018). Analysis of Swarm satellites data showing seismo-ionospheric anomalies around the time of the strong Mexico (Mw= 8.2) earthquake of 08 September 2017. *Advances in Space Research* 62 (3): 614-623. doi: 10.1016/j.asr.2018.04.043
- Marchetti D, De Santis A, D'Arcangelo S, Poggio F, Jin S et al. (2020). Magnetic field and electron density anomalies from Swarm satellites preceding the major earthquakes of the 2016–2017 Amatrice-Norcia (Central Italy) seismic sequence. *Pure and Applied Geophysics* 177 (1): 305-319. doi: 10.1007/s00024-019-02138-y
- Mavroulis S, Triantafyllou I, Karavias A, Gogou M, Katsetsiadou KN et al. (2021). Primary and secondary environmental effects triggered by the 30 October 2020, Mw= 7.0, Samos (Eastern Aegean Sea, Greece) earthquake based on post-event field surveys and InSAR analysis. *Applied Sciences* 11(7), 3281. doi: 10.3390/app11073281
- Mayaud PN (1980). Derivation, meaning, and use of geomagnetic indices. Washington DC American Geophysical Union Geophysical Monograph Series 22: 607. doi: 10.1029/GM022
- Oruç B, Balkan E (2021). Stress field estimation by the geoid undulations of the Samos-Kuşadası Bay and implications for seismogenic behavior. *Acta Geophysica* 1-13. doi: 10.1007/s11600-021-00604-7
- Pamukcu O, Yurdakul A (2008). Isostatic compensation in western Anatolia with estimate of the effective elastic thickness. *Turkish Journal of Earth Sciences* 17 (3): 545-557.
- Paréjas E (1940). La tectonique transversale de la Turquie. *Istanbul Üniversitesi Fen Fakültesi Mecmuası* 8: 244
- Parrot M (1995). Use of satellites to detect seismo-electromagnetic effects. *Advances in Space Research* 15 (11): 27-35. doi: 10.1016/0273-1177(95)00072-M
- Pulinets SA, Legen'ka AD, Alekseev VA (1994). Pre-earthquake ionospheric effects and their possible mechanisms. *Dusty and Dirty Plasmas, Noise, and Chaos in Space and in the Laboratory*. Boston, the USA: Springer.
- Pulinets S, Ouzounov D (2011). Lithosphere–Atmosphere–Ionosphere Coupling (LAIC) model–An unified concept for earthquake precursors validation. *Journal of Asian Earth Sciences* 41 (4-5): 371-382. doi: 10.1016/j.jseae.2010.03.005
- Pulinets SA, Ouzounov DP, Karelin AV, Davidenko DV (2015). Physical bases of the generation of short-term earthquake precursors: A complex model of ionization-induced geophysical processes in the lithosphere-atmosphere-ionosphere-magnetosphere system. *Geomagnetism and Aeronomy* 55 (4): 521-538. doi: 10.1134/S0016793215040131
- Ring U, Willner AP, Lackmann W (2001). Stacking of nappes with different pressure-temperature paths: An example from the Menderes nappes of western Turkey. *American Journal of Science* 301 (10): 912-944. doi: 10.2475/ajs.301.10.912
- Robertson AHF, Dixon JE (1984). Introduction: aspects of the geological evolution of the Eastern Mediterranean. *Geological Society, London, Special Publications* 17 (1): 1-74.
- Rostoker G (1972). Geomagnetic indices. *Reviews of Geophysics* 10 (4): 935-950. doi: 10.1029/RG010i004p00935
- Schermer ER, Lux DR, Burchfiel BC. (1990). Temperature-time history of subducted continental crust, Mount Olympos Region, Greece. *Tectonics* 9 (5): 1165-1195. doi: 10.1144/GSL.SP.1984.017.01.02
- Seidel E, Kreuzer H, Harre W (1982). A late Oligocene/early Miocene high pressure belt in the external Hellenides. *Geologisches Jahrbuch. Reihe E, Geophysik* (23): 165-206.
- Şengör AC, Yılmaz Y (1981). Tethyan evolution of Turkey: a plate tectonic approach. *Tectonophysics* 75 (3-4): 181-241. doi: 10.1016/0040-1951(81)90275-4
- Sorokin VM, Chmyrev VM, Yaschenko AK (2001). Electrodynamical model of the lower atmosphere and the ionosphere coupling. *Journal of Atmospheric and Solar-Terrestrial Physics* 63 (16): 1681-1691. doi: 10.1016/S1364-6826(01)00047-5
- Sugiura M, Poros DJ (1971). Hourly values of equatorial Dst for the years 1957 to 1970. NASA: Goddard Space Flight Center.
- Triantafyllou I, Gogou M, Mavroulis S, Lekkas E, Papadopoulos GA et al. (2021). The Tsunami Caused by the 30 October 2020 Samos (Aegean Sea) Mw7. 0 Earthquake: Hydrodynamic features, source properties and impact assessment from post-event field survey and video records. *Journal of Marine Science and Engineering* 9 (1): 68. doi: 10.3390/jmse9010068
- Tronin AA, Hayakawa M, Molchanov OA (2002). Thermal IR satellite data application for earthquake research in Japan and China. *Journal of Geodynamics* 33 (4-5): 519-534. doi: 10.1016/S0264-3707(02)00013-3
- Troyan VN, Hayakawa M (2002). Seismo Electromagnetics: Lithosphere-Atmosphere-Ionosphere Coupling. In *Seismo Electromagnetics: Lithosphere-Atmosphere-Ionosphere Coupling*. Tokyo, Japan: Terra Scientific Publishing Company. pp. 215-221.
- Vallianatos F, Pavlou K (2021). Scaling properties of the Mw7. 0 Samos (Greece), 2020 aftershock sequence. *Acta Geophysica* 1-18. doi: 10.1007/s11600-021-00579-5
- Vizzini F, Brai M (2012). In-soil radon anomalies as precursors of earthquakes: a case study in the SE slope of Mt. Etna in a period of quite stable weather conditions. *Journal of Environmental Radioactivity* 113: 131-141. doi: 10.1016/j.jenvrad.2012.05.027
- Walcott CR (1998). The alpine evolution of Thessaly (NW Greece) and late Tertiary Aegean kinematics 162: 1-176.
- Zhu K., Li K, Fan M, Chi C, Yu Z (2019). Precursor Analysis Associated With the Ecuador Earthquake Using Swarm A and C Satellite Magnetic Data Based on PCA. *IEEE Access* 7: 93927-93936. doi: 10.1109/ACCESS.2019.2928015